Multimodal Analysis of Oak Wood Metabolites for a Comprehensive Understanding of the Aging Process in Typical French Spirit Barrels

Aline Cournut, Quentin P. Vanbellingen, Anaïs Demaye, Matthias Ochs, Andreas Römpp, David Touboul, Véronique Eparvier, Alain Brunelle

Multimodal Analysis of Oak Wood Metabolites for a Comprehensive Understanding of the Ageing Process in typical French Spirit Barrels

Aline Cournut[a+], Quentin P. Vanbellingen[a+†], Anaïs Demaye[b], Matthias Ochs[c], Andreas Römpp[c], David Touboul[d], Véronique Eparvier[b], Alain Brunelle[a*]

[a]Sorbonne Université, CNRS, Laboratoire d'Archéologie Moléculaire et Structurale (LAMS), Paris, France

[b]Université Paris-Saclay, CNRS, Institut de Chimie des Substances Naturelles, UPR 2301, Gif-sur-Yvette, France

[c]University of Bayreuth, Bioanalytical Sciences and Food Analysis, Bayreuth, Germany

[d]Ecole Polytechnique, CNRS, Laboratoire de Chimie Moléculaire, Institut Polytechnique de Paris, Palaiseau, France

ABSTRACT: Oak wood plays a crucial role in barrel ageing, significantly influencing the flavor, aroma, and quality of aged spirits. This study integrates Liquid Chromatography-Tandem Mass Spectrometry (LC-MS/MS), Laser Desorption/Ionization Mass Spectrometry (LDI-MS) and Time-of-Flight Secondary Ion Mass Spectrometry (TOF-SIMS) to analyze metabolite distribution in oak wood. By comparing freshly cut wood, freshly toasted wood, or historical wood staves of 2- 50- or 100-year-old, this multimodal approach reveals spatial distribution changes in lignin, polysaccharides, lipids, and extractable compounds such as phenolic ones. Notably, the degradation of polysaccharides and migration of ellagitannins are observed, providing new insights into wood-ageing dynamics. These findings offer potential improvements in barrel ageing techniques to enhance the sensory profile of spirits.

INTRODUCTION

Oak wood (*Quercus spp.*) plays a major role in the maturation of distilled spirits, specifically in the production of high-quality beverages like whisky or Cognac. Oak barrels serve not only as a storage medium but also as a reactive vessel where complex chemical interactions take place between the wood's molecular components and the liquid. These interactions impart distinct characteristics, including flavor, color, and mouthfeel, which define the quality of the final product.[1,2] The molecular identity of oak, particularly its lignin's, polysaccharides, phenolic compounds, and lipids, is essential in shaping the organoleptic properties of the matured spirits,[3] each of these compounds having a specific function in spirit maturation.[4]

Lignins are complex polymers that provide structural support and rigidity to the wood. Derived from three main monolignols – *p*-coumaryl alcohol, coniferyl alcohol, and sinapyl alcohol – they form the building blocks of different lignin units: H (hydroxyphenyl), G (guaiacyl), and S (syringyl). These lignin types have distinct distributions across different cell types within the oak, contributing to the wood's mechanical properties. During barrel ageing, lignins are believed to influence the oxidative stability of the maturing spirits and contribute to the formation of aromatic compounds such as vanillin through thermal degradation during barrel toasting.[5]

Oak wood contains abundant polysaccharides, including cellulose and hemicellulose, which form the structural framework of plant cell walls. Cellulose provides tensile strength, while hemicellulose serves as a matrix that supports cellulose fibers.[5] During barrel ageing, the partial hydrolysis of these polysaccharides contributes to the release of sugars, which can influence the sweetness of spirits. However, long-term ageing, environmental exposure, and alcohol interaction can lead to polysaccharide degradation, altering the wood's structural integrity and impacting flavor extraction.

Phenolic compounds are critical in oak wood for their antioxidant properties and significant contribution to the aroma, flavor, and color of the spirits.[3,6] These include simple phenols (e.g., *vanillin*, *syringaldehyde*) and more complex tannins, such as ellagitannins.[7] Ellagitannins, in particular, are unique to oak wood and play a protective role in the tree, acting as a defense against pathogens.[4] During barrel ageing, ellagitannins degrade into ellagic acid, which can impart color, astringency and bitterness to the liquors.[8,9] Understanding the distribution and transformation of these compounds is a key to manage the flavor profile during spirits maturation.

Lipids, including fatty acids and sterols, are essential components of oak wood, playing a role in the ageing process by interacting with alcohol, which may lead to the release of free fatty acids into the spirits. This release can affect the texture and taste of the beverage. Long-term ageing can result in the degradation or extraction of these lipid components, altering the chemical properties of the barrel.

The chemical complexity and diversity of oak wood is a significant challenge to researchers. While several studies have focused on the contribution of specific compounds to the ageing process, there is still a limited understanding of how these compounds are distributed and how their spatial arrangement evolves over time. Furthermore, the interaction between the different wood metabolites and the maturing spirits remains underexplored. A multimodal approach, combining advanced analytical techniques like Time-of-Flight Secondary Ion Mass Spectrometry (TOF-SIMS) imaging, Laser Desorption Ionization Mass Spectrometry (LDI-MS) and Liquid Chromatography coupled with Tandem Mass Spectrometry (LC-MS/MS), offers a novel perspective on this topic. TOF-SIMS enables the high-resolution imaging of metabolite distribution within wood structures, such as the wood rays, while LC-MS/MS focuses

on identifying specific wood metabolites and their chemical transformations. LDI-MS provides data with high mass accuracy which supports compound annotation directly on the wood sample and therefore bridges the results from TOF-SIMS and LC-MS/MS. By integrating these methods, we aim to map the spatial dynamics of central and specialized metabolites in freshly cut wood, freshly toasted wood (t_0) and historical wood of 2- 50- or 100-year-old oak staves (t_2, t_{50}, and t_{100}) used in barrel ageing, providing deeper insights into the chemical processes that govern the evolution of wood metabolites during ageing.

EXPERIMENTAL SECTION

Wood Staves

Different types of samples, representing various stages in the life of an oak barrel, were collected from a cooperage, and from the barrel repair workshop of a major Cognac brand. The first ones include samples of staves, which are pre-cut oak wood in pallet form. These were analyzed based on several criteria: (1) fresh staves (i) with fine grain (ii) with coarse grain; (2) mature staves (i) with fine grain (ii) with coarse grain. Mature staves refer to wood that has aged outdoors for two years, near the cooperage building, under natural climatic conditions. After this ageing process, the mature staves are used to manufacture the barrels. The staves are shaped into barrel form and then toasted to eliminate unwanted compounds that could negatively impact the colors and aromas of the ageing spirits. The second group of analyzed samples from the barrel repair workshop consists of barrel staves that have been 2, 50 and 100 years long in contact with alcohol. The 0-year mark indicates barrels that have never been in contact with alcohol, and was provided by the cooperage, from toasted staves that broke during assembly of the barrel.

LC-MS/MS Sample Preparation

Stave samples were ground into fine wood shavings using a grinder (Waring Laboratory Science Blender, Torrington, USA). These shavings were macerated in 96% ethanol for 48 hours under slow agitation. The ethanol extracts were filtered and dried using a rotary evaporator at 35°C, and stored at 5°C. The dried extracts were dissolved in absolute ethanol (Sigma-Aldrich, Saint-Quentin-Fallavier, France) to a concentration of 1 mg/mL, filtered through PTFE filters, and transferred into vials for LC-MS/MS analysis.

TOF-SIMS Sample Preparation

Stave samples were cut into small blocks (approximately 25 × 3 × 2.5 mm) using a scroll fret saw. The blocks were then cut with a microtome (HistoCore Multicut R, Leica, France) equipped with a carbon steel knife to obtain a flat surface suitable for ion beam analysis. For this, they were mounted on micro-vices specially manufactured in the laboratory's mechanical workshop, in order to maintain the parallelism of the sample surface with the TOF-SIMS holder, from cutting with the microtome to mounting on the latter.

LC-MS/MS Analysis

LC-MS/MS was conducted using a LC 1260 Prime (Agilent Technologies, Santa Clara, CA 95051, USA) system coupled to a 6540 Q-TOF mass spectrometer (Agilent Technologies, Santa Clara, CA 95051, USA) equipped with a reverse phase CORTECS T3 column, 90 Å, 1.6 µm, 2.1 mm × 50 mm (Waters). Mobile phases consisted of water + 0.1% formic acid (A) and acetonitrile (B). The gradient started at 5% B and increased to 100% B over 18 minutes. The flow rate was set at 0.4 mL.min^{-1}. The oven was heated to 45°C. Injection volume was fixed at 5 µL. Mass spectrometry analyses were performed using an electrospray source in both positive and negative modes. The MS parameters were as follows: gas temperature 325°C, gas flow 10 L.min^{-1}, nebulizer pressure 30 psi, sheath gas temperature 350°C, sheath gas flow 10 L.min^{-1}, capillary voltage 3500 V, nozzle voltage 500 V, fragmentor voltage 110 V, skimmer voltage 45 V, octopole RF Peak 750 V. The four most intense ions in MS were selected for MS/MS with an absolute intensity threshold of 1000 a.u. The selected precursor ions were fragmented at a collision energy of 20 eV.

LDI-Orbitrap Analysis

LDI-MS experiments were performed using an AP-SMALDI5 AF (TransMIT GmbH, Gießen, Germany) atmospheric pressure MALDI imaging source coupled to a Q Exactive HF (Thermo Fisher Scientific, Bremen, Germany) orbital trapping mass spectrometer. No matrix was applied to the wood samples, which were prepared as for the TOF-SIMS analyses. For MS data acquisition the Thermo software Q-Exactive- HF tune Version 2.9 was used and the LDI source was controlled by the provided TransMIT software Master Control Program Version 3.9. Measurements were conducted with 30 laser shots per pixel and a mass range of *m/z* 100-400 with a step size of 50 µm × 50 µm, in both positive and negative modes.

TOF-SIMS Analysis

TOF-SIMS experiments were conducted using a TOF-SIMS IV mass spectrometer (IONTOF GmbH, Münster, Germany) equipped with a liquid metal ion gun (LMIG) that delivers a pulsed Bi_n^{q+} ion beam (with n = 1-7 and q = 1 or 2). Bismuth ions impact the sample with a kinetic energy of 25 q.keV at an incidence angle of 45°. All experiments were conducted selecting Bi_3^+ clusters using dual blanking plates. The resulting secondary ions were accelerated to a kinetic energy of 2 keV (2 kV extraction) towards a field free region and a single stage reflector (first order compensation). The secondary ions were post-accelerated to a kinetic energy of 10 keV before hitting a hybrid detector composed of a microchannel plate, a scintillator, and a photomultiplier. Between two successive primary ion pulses, a low energy electron gun (~20 eV) was used to neutralize the sample surface. Pulsed primary ion currents were measured with a Faraday cup located on the grounded sample holder. To profile ion intensity along stave thickness, analyses were carried out in high current bunched (HCBU) mode[10] with a lateral resolution of about ~2 µm, a mass resolution power of $m/\Delta m$ ~5,000 at *m/z* 430, using a fluence of about ~4×10^{11} ions.cm^{-2} under a Bi_3^+ current of about ~0.4 pA. Each measurement for the profile was done by recording an ion image of 500 µm × 500 µm surface, and recording the total counts of the selected ions over the whole image surface. Successive images were recorded each 0.5 mm along the 25 mm stave thickness, from one side to the other.

Mass spectra and ion images were recorded in both positive and negative modes. Due to the very low initial distribution of the kinetic energies of the secondary ions, the relationship between the flight time and the square root of the *m/z* value is always linear across the entire mass range. Mass calibration was always internal, and the signals used for the initial calibration were those of C^+, CH_2^+, CH_3^+ $C_2H_3^+$, $C_2H_5^+$, $C_3H_3^+$ and $C_3H_5^+$ for the positive polarity mode and those of C^-, CH^-, CH_2^-, CH_3^-, C_2^-, C_3^-, C_4H^- for the negative polarity mode.

To measure ion distributions at subcellular resolution, acquisitions were performed in burst alignment mode coupled to a delayed extraction of secondary ions (BA-DE)[11]. Lateral resolution reached 400 nm and mass resolution

m/Δm ~7,000 at *m/z* 430. In this mode low *m/z* ions are accelerated at a kinetic energy lower than heavier *m/z* ions. For this reason, the relationship between the flight time and the square root of the *m/z* value is not linear. To provide accurate calibration, spectra were calibrated using $C_7H_7^+$, $C_9H_9^+$, *etc.*[12]

LC-MS/MS Data Processing

LC-MS/MS data were first processed using MassHunter Qualitative Analysis 10.0 (Agilent Technologies, Santa Clara, CA 95051, USA). The data files were then converted from the .d standard data format (Agilent Technologies) to .mzXML format using the MSConvert software, part of the ProteoWizard package 3.0[13]. All .mzXML were processed using MZmine2v53 as previously described[14]. The mass detection was realized with MS1 noise level at 1000 and MS/MS noise level at 50. The ADAP chromatogram builder was employed with a minimum group size of scans of 3, a group intensity threshold of 1000, a minimum highest intensity of 1000, and *m/z* tolerance of 0.008 (or 20 ppm). Deconvolution was performed with the ADAP wavelets algorithm according to the following settings: S/N threshold = 10, minimum features height = 1000, coefficient/area threshold = 10, peak duration range 0.01 – 1.5 min, t_R wavelet range 0.00 – 0.04 min. MS/MS scans were paired using an *m/z* tolerance range of 0.05 Da and t_R tolerance range of 0.5 min. Isotopologues were grouped using the isotopic peak grouper algorithm with an *m/z* tolerance of 0.008 (or 20 ppm) and a t_R tolerance of 0.2 min. Peaks were filtered using Feature list row filter, keeping only peaks with MS/MS scans. Peak alignment was performed using the join aligner with an *m/z* tolerance of 0.008 (or 20 ppm), and a retention time tolerance of 0.2 min. The MGF file and the metadata were generated using the export/submit to molecular network option. Molecular networks using the t-SNE (t-distributed stochastic neighbor embedding) algorithm were calculated and visualized using MetGem 1.4.3 software[15]. MS/MS spectra were window-filtered by choosing only the top 6 peaks in the ± 50 Da window throughout the spectrum. The data were filtered by removing all peaks in the ± 17 Da range around the precursor *m/z*. The *m/z* tolerance windows used to find the matching peaks was set to 0.04 Da and the minimum matched peak was set to 2. The cosine score between two MS/MS spectra was set at 0.5. The number of iterations was 10000, the perplexity was 6, the learning rate was 10 and the early exaggeration was set to 12, Barnes-Hut approximation was used. Peaks were aligned and matched with spectral databases to identify the compounds. Database search was performed according to the following parameters: *m/z* tolerance 0.02; Minimum Matched Peaks 2; Minimal Intensity 0 %; *m/z* parent Filter Tolerance 17; Minimal Cosine Score Value 0.40. Node size was set by the sum of the amount of ion in each sample for that node.

TOF-SIMS Data Processing

The TOF-SIMS raw data, acquired with SurfaceLab 6.8 software, were converted and processed using SurfaceLab 7.4 (IONTOF GmbH, Münster, Germany). Regions of interest (ROI) were drawn based on wood areas from the overlay of optical images (for example, rays, fibers, and parenchyma cells).

LDI-MS Data Processing

MS spectra were analyzed using the proprietary software Xcalibur 4.0 from Thermo Fisher Scientific. Thermo RAW files were converted to the imzML format (imzML Converter Version 2.0.4) for processing with the in-house tool imzmlAnalyzer for initial quality control.

RESULTS AND DISCUSSION

LC-MS/MS analysis and molecular network visualization.

t-SNE molecular network visualization in both negative (Figure 1) and positive (Figure 2) ionization modes allowed the annotation of several classes of molecules distributed across the network in ten or twelve clusters, respectively. Each of those clusters allowed the annotation of specific metabolite from the oak wood. The Table S1 and Table S2 from the supporting information summarizes the different compounds annotated by LC-MS/MS analysis using t-SNE molecular network visualization. All compounds were annotated using reference about wood composition[1–8,16–19], the t-SNE visualization, the SIRIUS software to annotate the corresponding chemical formula and the respective fragmentation mass spectra from the compound (Figure S1 to Figure S14).

The seven classes of molecules annotated in negative ionization mode (Figure 1) are composed of two clusters of triterpenoids, one cluster of lipids, one cluster of gallotanins, one cluster of other galloyl compounds, two clusters of lignans, one cluster of coumarins and one cluster of small molecular weight phenolic compounds. The latter being the most abundant ones in the molecular network view as pinpointing by the circumference of the node in the phenol cluster. All the corresponding annotated compounds can be found in Table S1 of Supporting Information.

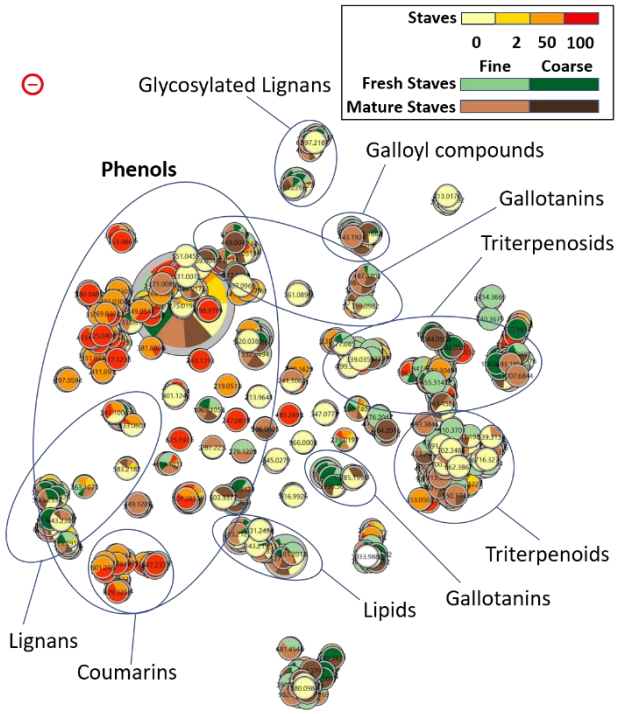

Figure 1: Molecular network t-SNE visualization of LC-MS/MS analysis in negative ionization mode for eight different wood samples (fine and coarse grain fresh and mature staves, staves that have been in contact during 0, 2, 50 and 100 years with alcohol – t0, t2, t50, t100).

The nine classes of molecules annotated in positive ionization mode (Figure 2) are composed of one cluster of triterpenoids, one cluster of lipids, two clusters of gallotanins, two clusters of lignans, one cluster of flavonoids, one cluster of polyketones, one cluster of alkaloids, one cluster of glycol compounds and two clusters of small molecular weight phenolic compounds. The latter being the most abundant ones in the molecular network view as pinpointing by the circumference of the node in the bottom phenol cluster. It is important to notice here that the positive ionization mode allowed the annotation of more classes of

molecules than the negative ionization mode. Flavonoids, polyketones, and alkaloids are then added to the annotated molecular groups. All the corresponding annotated compounds for the positive ionization mode can be found in Table S2 of Supporting Information.

Gallotanins

Ellagic acid, a key metabolite for its contribution to astringency and oxidative stability in spirits, was detected at *m/z* 300.9973 (Δm = 5.65 ppm) $[M-H]^-$ in all stave and barrel samples (Figure 1 and Figure S1). However, a derivative of ellagic acid (*m/z* 275.0196 Δm = 0.364 ppm in negative ionization mode, molecular formula $C_{13}H_8O_7$) showed intensity increase linked to toasting and alcohol exposure stages (Figure S3). Initially, the intensity of this derivative increased after toasting, indicating that the heat applied during this stage promotes the release or formation of certain ellagic acid derivatives. After 50 years of contact with alcohol (t_{50}), its intensity returned to baseline, suggesting progressive extraction through time or even possibly to the degradation of the molecules under long-term alcohol storage. This suggests that toasting temporarily increases certain gallotannins levels, but barrel ageing (after toasting at t_0 from t_{100}), particularly through alcohol exposure, gradually reduces these compounds.

Additionally, two specific derivatives of ellagic acid, $C_{15}H_8O_8$ (methylated ellagic acid) and $C_{14}H_4O_8$ (dehydroxylated ellagic acid), were only annotated in barrel samples that had 100 years of alcohol exposure (Figure S4). As depicted by Viriot *et al.*, this result implies that long alcohol contact drives to ellagitannins degradation[17] leading to alteration in astringency and bitterness of the aged spirits[4].

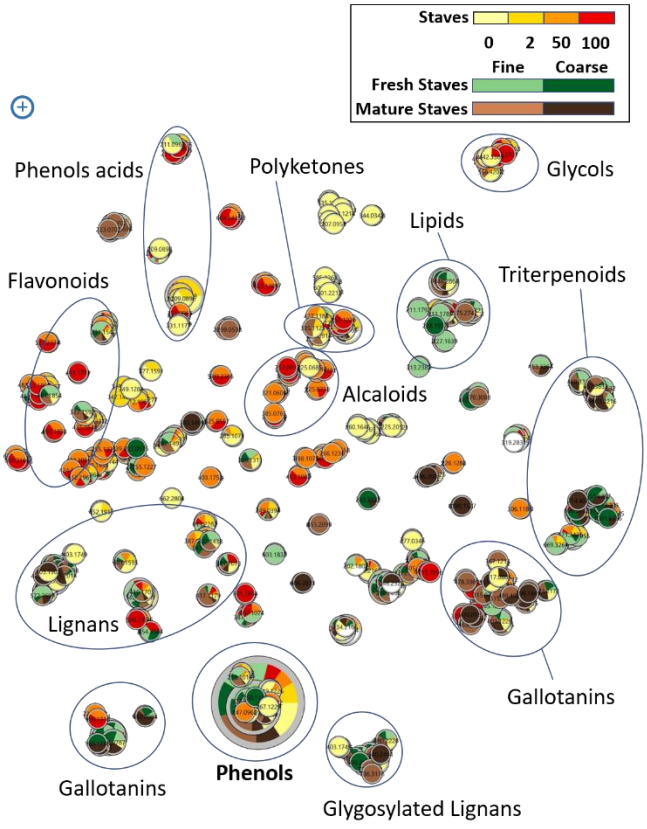

Figure 2: Molecular network t-SNE visualization of LC-MS/MS analysis in positive ionization mode of eight different wood samples (fine and coarse grain fresh and mature staves, staves that have been in contact during 0, 2, 50 and 100 years with alcohol – t_0, t_2, t_{50}, t_{100}).

Moreover, other types of gallotanins were annotated using the positive ionization mode (Figure 2). The different annotated gallotannins (gallic acid derivatives and ellagic acid derivatives) are mainly found in fresh and mature wood samples, indicating a significant impact of toasting on the degradation of these compounds, implying that gallotanins could have different behavior to toasting or alcohol ageing depending on their structures.

Vescalagin or castalagin[20,21] (*m/z* 933.0636 Δm = 0.429 ppm, $C_{41}H_{26}O_{26}$) was present in all samples (negative ionization mode) and showed resistance to the toasting stage (Figure 1 and Figure S5). However, their intensity decreased over ageing, showing a tenfold reduction between samples t_2 and t_{100}. In the same way, positive ionization mode results (Figure S6) showed that the two isomers[20,21] (*m/z* 935.0787 Δm = -0.214 ppm) were also present in fresh and mature stave samples, as well as in barrel samples t_0, t_2, and t_{50}. However, in this case, a decrease in castalagin/vescalagin intensity with prolonged alcohol contact results in the compound complete disappearance at t_{100}. This reduction – or disappearance – is likely due to vescalagin and castalagin solubility in alcohol, thus facilitating their gradual extraction into the spirit through time.

Ethyl derivatives[21] (Figure 1 and Figure S5, *m/z* 961.0944 Δm = 0.936 ppm, $C_{43}H_{30}O_{26}$) of these compounds, identified in all samples but in lower quantities, or oxidized castalagin/vescalagin (Figure 2 and Figure S6), identified only after 50 years of alcohol contact, could represent forms modified by the reaction with the ethanol contains in the barrel. In the same way, castalin/vescalin molecules[21] (Figure 2 and Figure S6) are found in fresh and mature staves and appear under oxidized form after 50 or 100 years of alcohol contact.[9]

This reveals that alcohol not only extracts gallotannins but also facilitates their partial ethylation and/or oxidation, leading to a potential modification of the taste profiles of the ageing spirit.

Lactones such as open glucoside lactone (*m/z* 335.1688 Δm = 6.86 ppm, $C_{15}H_{28}O_8$) and open rutinoside lactone (*m/z* 481.2269 Δm = 4.57 ppm, $C_{21}H_{38}O_{12}$) were detected[22] in fresh or mature staves and t_0 samples but were not detected in aged samples (t_2, t_{50}, and t_{100}), suggesting that alcohol contact is a major factor in their total degradation or disappearance (Figure 1, Figure S7 and Figure S8). Moreover, in the positive ionization mode (Figure 2), the same behavior can be noticed from the class of galloyl compounds. Indeed, several galloyl compounds are identifiable in all fresh and mature samples and in the t_0 barrel sample (open galloylglucoside lactone[22,23] *m/z* 489.1969 Δm = −0.409 ppm, $C_{22}H_{32}O_{12}$, *m/z* 523.2174 Δm = 0 ppm, $C_{26}H_{34}O_{11}$ and *m/z* 525.2328 Δm = 0.381 ppm, $C_{26}H_{36}O_{11}$,), implying once again that the toasting stage has no effect on these compounds, but that prolonged alcohol contact leads to their extraction from the wood or even possibly to their degradation inside the wood.

Lignans and Phenolic Acids

Different behaviors are observed depending on the lignan species. Lyoniresinol[24,25] (*m/z* 419.1689 Δm = 5.25 ppm, $C_{22}H_{28}O_8$) (Figure 1 and Figure S9) and syringaresinol[24,25] (*m/z* 419.1701 Δm = −0.239 ppm, $C_{22}H_{26}O_8$) (Figure 2) were detected[26] with no difference of amount across all samples, showing remarkable stability despite toasting or alcohol exposure duration. This may be due to its structure, thus enabling this type of lignans to resist extraction by alcohol. On the other hand, scorzonoside[27], detected at *m/z* 568.2390

Δm = −42.2 ppm (Figure 2, $C_{27}H_{36}O_{13}$), was solely identified after 50 or 100 years of alcohol contact, demonstrating a tendency for alcohol extraction through prolonged ageing.

Phenolic acids, identified only in barrel samples, indicate their formation and therefore thee possibility to detect them after the toasting. For example, sinapaldehyde[25] (Figure 1 and Figure S10 *m/z* 207.0647 Δm = 7.73 ppm or Figure 2 *m/z* 209.0813 Δm = 2.39 ppm)[28] showed a progressive decrease in intensity during ageing, especially after 50 years of contact with alcohol. Thus, heat seems to promote the initial release of these compounds, while alcohol solubility leads to their long-term reduction.

Triterpenoids and Lipids

Arjungenin[29] (*m/z* 503.3377 Δm = 0.199 ppm, $C_{30}H_{48}O_6$), which is detected across all samples, showed initial stability but progressively degraded with prolonged ageing (Figure 1 and Figure S11). Derivatives (Bartogenic acid/robural A *m/z* 517.3163 Δm = 1.55 ppm and Bellericagenin B *m/z* 519.3316 Δm = 2.12 ppm)[30–32] appeared after two years of alcohol contact, suggesting that ageing gradually modifies the structure of triterpenoids through successive degradation and transformation mechanisms. In the positive ionization mode (Figure 2) this tendency is pinpointed by a detection of the terpenoid class solely in the fresh and mature stave or the t_0 sample. Thus, implying degradation during long-term contact with alcohol.

Fatty acid like $C_{18}H_{34}O_5$ (*m/z* 329.2334 Δm = -0.304 ppm) were detected in all samples (Figure S14) but its intensity decreased with alcohol contact. This behavior was also observed for other fatty acids, including those with *m/z* 301.2018 Δm = 0.996 ppm ($C_{16}H_{30}O_5$), *m/z* 331.2491 Δm = −0.302 ppm ($C_{18}H_{36}O_5$), *m/z* 327.2173 Δm = 1.22 ppm ($C_{18}H_{32}O_5$), and *m/z* 343.2119 Δm = 2.04 ppm ($C_{18}H_{32}O_6$). This suggests that alcohol, due to its solvent properties, causes a gradual extraction of lipids, reducing their quantity in the oldest barrel samples (t_{50} and t_{100}). Some fatty acids less affected by alcohol contact were also identified, showing that some lipids remain stable, potentially playing a role in preserving the texture and hydrophobic barrier property of the wood. Moreover, the glycol compounds demonstrate the same behavior when analyzed with the positive ionization mode. Indeed, in this case, the multiple detected glycolated compounds (*m/z* 249.2061 Δm = -0.401 ppm ($C_{13}H_{28}O_4$), *m/z* 251.1853 Δm = 0 ppm ($C_{12}H_{26}O_5$), *m/z* 309.2270 Δm = 0.647 ppm ($C_{15}H_{32}O_6$), *m/z* 384.2958 Δm = -0.520 ppm ($C_{18}H_{38}O_7$), *m/z* 442.3374 Δm = 0 ppm ($C_{21}H_{44}O_8$), *m/z* 500.3793 Δm = 0 ppm ($C_{24}H_{50}O_9$)) were only identifiable in barrel samples, starting t_0. Here, the compound intensity increased with the duration of alcohol contact, suggesting their role for wood via a hydrophobic barrier.

The results obtained through LC-MS/MS combined with molecular networking visualization enabled the annotation of a total of 66 molecules. These findings also highlighted the impact of the toasting process on the various categories of identified molecules, as well as the effect of prolonged contact between wood and alcohol on wood-derived molecules. Based on these results, it can be concluded that the most relevant wood samples for elucidating the ageing process of spirit and its influence on wood molecules are those taken after toasting (t_0, t_2, t_{50}, and t_{100}). Moreover, while comparisons across all four samples revealed general trends, only the comparison between t_0 and t_{100} samples demonstrated statistically significant differences. Consequently, the following TOF-SIMS analyses focused on the t_0 and t_{100} stave samples.

TOF-SIMS profiling and imaging to visualize the specific spatial distribution through the t0 and t100 stave samples.

TOF-SIMS analysis in both ionization modes allowed the annotation and the specific spatial localization of metabolite from the oak wood. The Tables S5 and S6 from the supporting information summarizes the compounds detected and annotated by TOF-SIMS.

Lignin Distribution in Fresh and Aged Oak

Lignins are essential components of the wood structure, providing mechanical strength, and contributing to the oxidative stability of the spirits during ageing.

TOF-SIMS analysis revealed the spatial distribution of lignin monomers – H-lignin, G-lignin, and S-lignin – in freshly toasted oak (Figure 3)[33,34] and its ion profiles along the cross section of both freshly toasted (t_0) and aged oak staves (t_{100}) (Figure 4, Figure S15). All lignins ions annotation were made according to Saito *et al.*, and Goacher *et al.* published reference spectra[34,35].

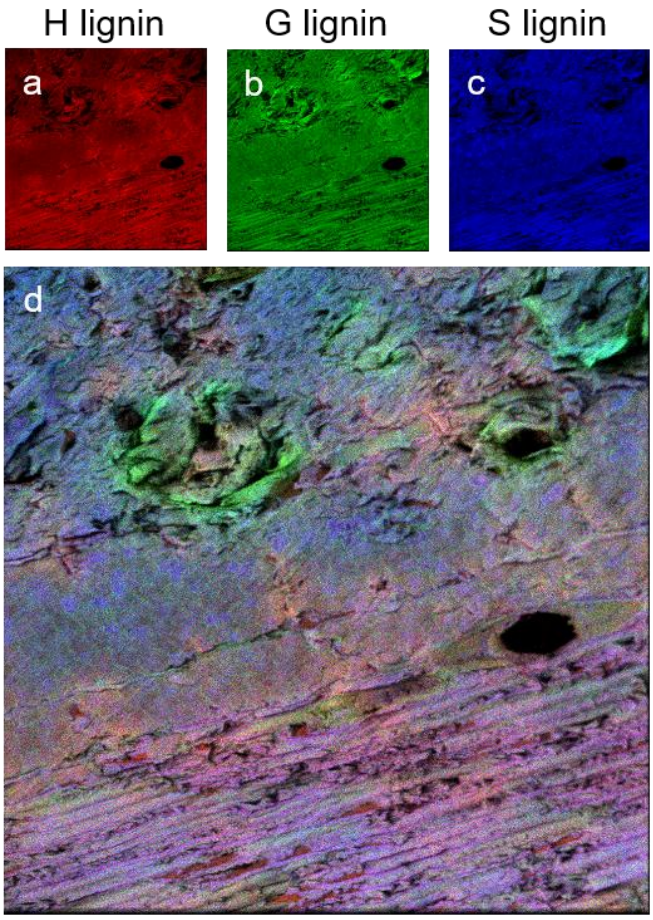

Figure 3: High spatial resolution TOF-SIMS images of a freshly toasted sample wood (t_0) cross section recorded in BA-DE mode (image size 400 µm × 400 µm, 1024 × 1024 pixels, pixel size 0.4 µm, primary ion dose density 4.10^{12} ions.cm^{-2}). a: S-lignin ions (*m/z* 167.07, $C_9H_{11}O_3^+$ and *m/z* 181.06, $C_9H_9O_4^+$); b: G-lignin ions (*m/z* 137.06, $C_8H_9O_2^+$ and *m/z* 151.04, $C_8H_7O_3^+$); c: H-lignin ions (*m/z* 107.05, $C_7H_7O^+$ and *m/z* 121.03, $C_7H_5O_2^+$); d: 3-color overlay of a, b, and c images.

H-lignin (*m/z* 107.050 Δm = -9.34 ppm, $C_7H_7O^+$ and *m/z* 121.027 Δm = 8.26 ppm, $C_7H_5O_2^+$) was the most abundant across all wood cell types, particularly concentrated in the fiber cells. Its uniform distribution in both t_0 and t_{100} staves suggests that this lignin type remains relatively stable over time. The high abundance of S-lignin in fiber cells, which are responsible for the mechanical support

of the wood, aligns with its role in enhancing the wood's resistance to degradation, even after 100 years of ageing.

G-lignin (*m/z* 137.060 *Δm* = -2.19 ppm, $C_8H_9O_2^+$ and *m/z* 151.038 *Δm* = 6.62 ppm, $C_8H_7O_3^+$) and S-lignin (*m/z* 167.072 *Δm* = -12.0 ppm, $C_9H_{11}O_3^+$ and *m/z* 181.056 *Δm* = -33.1 ppm, $C_9H_9O_4^+$), on the other hand, exhibited more localized distributions. G-lignin was primarily detected in vessels containing tyloses – outgrowths that block vessels to prevent sap movement, potentially indicating a role in protecting these regions from microbial invasion. S-lignin was found mainly in parenchyma cells, which store and transport nutrients within the wood.

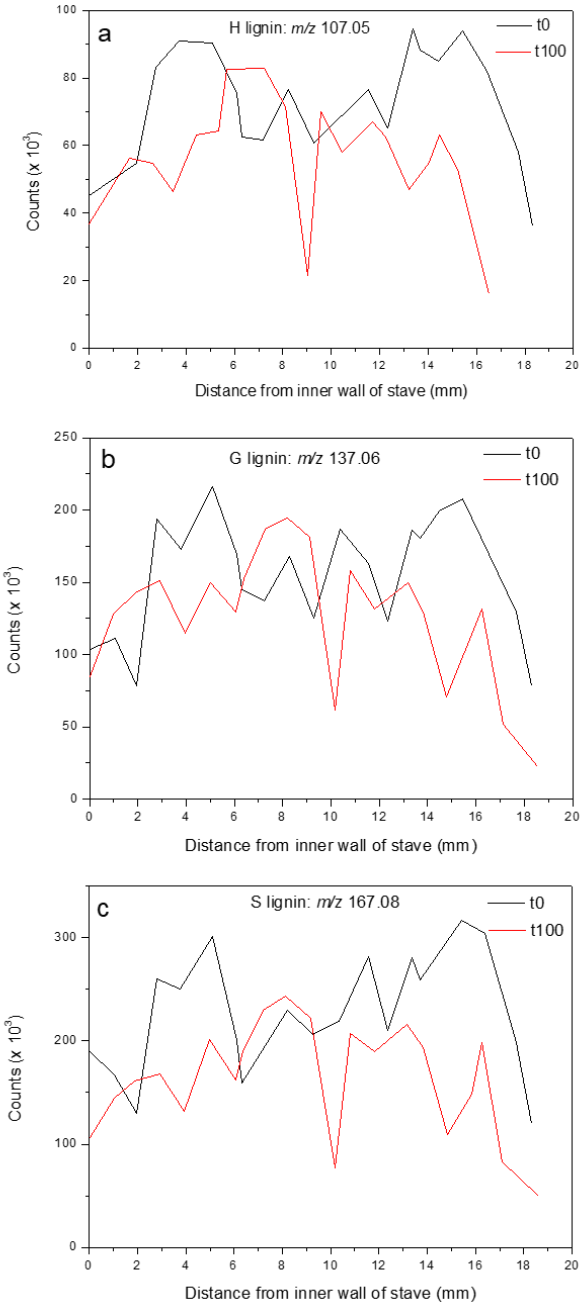

Figure 4: TOF-SIMS positive ion intensity profiles of lignin fragment ions, a *m/z* 107.05 (H lignin), b *m/z* 137.06 (G lignin), c *m/z* 167.07 (S lignin), recorded along stave cross sections. t0 (black) and t100 (red), 0 and 100 years contact with alcohol, respectively. Each measurement point is the mean value over measurements with 3 different samples. Error bars are not shown for the sake of clarity of the figure, and same profiles with error bars are shown in Supplementary Figure S16.

Overall, the findings suggest that while lignin is resistant to extensive degradation, the specific distribution of different lignin types may influence the structural and chemical properties of oak barrels over time. The persistence of lignin over 100 years implies its crucial role in maintaining the stave integrity and in contributing to the development of aromatic compounds that enrich the flavor of the aged spirits.

Wood sections were also analyzed by LDI mass spectrometry in profiling mode. In positive mode, the lignin signal discussed above could also be detected with accurate mass (typically better than 1 ppm). A mass spectrum for *m/z* 105 – 170 is shown in Figure S20. In this measurement S-lignin was detected at *m/z* 167.07030 (*Δm* = 0.18 ppm), G-lignin fragments were detected at *m/z* 137.05975 (*Δm* = 0.73 ppm) and *m/z* 151.07539 (*Δm* = 0.36 ppm) and H-lignin fragment was detected at *m/z* 107.04949 (*Δm* = 0.37 ppm). Initial experiments showed that the use of matrix compounds typically used for MALDI did not result in a significant increase of signal intensities. Therefore, measurements were performed in LDI mode (*i.e.* without use of matrix). Ionization efficiency for larger molecules decreased significantly, we therefore focused on the mass range up to *m/z* 400. Nevertheless, the high mass accuracy data of these LDI measurements provide valuable information to confirm the annotation of compounds directly on the wood section and to bridge the gap between LC-MS/MS and TOF-SIMS analyses. In combination this approach results in a high reliability of the identity of wood components reported in this study.

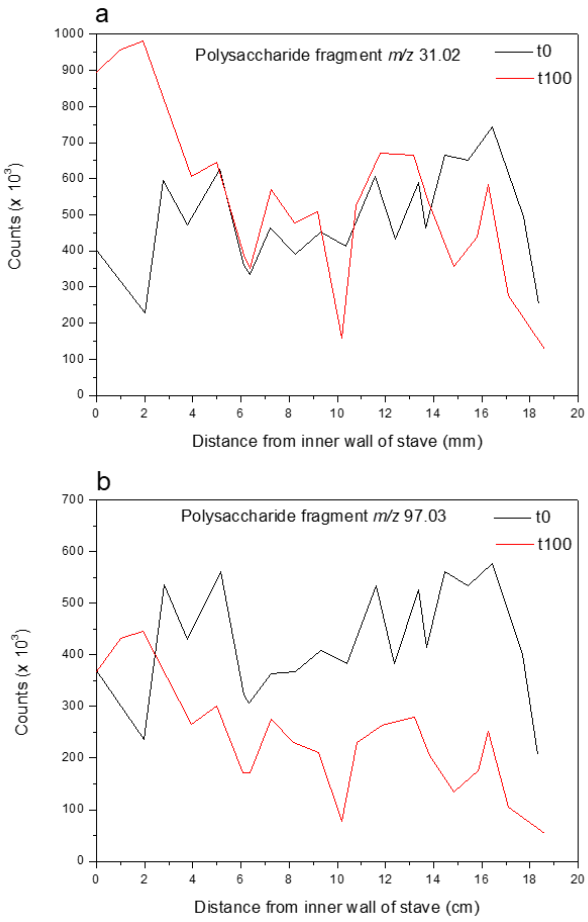

Figure 5: TOF-SIMS positive ion intensity profiles of polysaccharides fragment ions, a *m/z* 31.02 CH_3O, b *m/z* 97.03 $C_5H_5O_2$, recorded along stave cross-sections. t0 (black) and t100 (red), 0 and 100 years contact with alcohol, respectively. Each measurement point is the mean value over measurements with 3 different samples. Error bars are not shown for the sake of clarity of the figure, and same profiles with error bars are shown in Supplementary Figure S17.

Polysaccharide Degradation During Barrel Ageing

Polysaccharides, mainly cellulose and hemicellulose, are essential for the structural integrity of oak wood. TOF-SIMS imaging with high spatial resolution of freshly toasted staves showed a specific distribution of polysaccharides across the wood surface. Characteristic fragment ions for cellulose (*m/z* 127.041 *Δm* = -15.7 ppm, $C_6H_7O_3^+$) and hemicellulose (*m/z* 115.042 *Δm* = -26.1 ppm, $C_5H_7O_3^+$) were abundantly detected,[36] particularly in fiber cells, reflecting the high structural integrity of the freshly toasted wood (Figure S18)[33].

These two fragments were also confirmed by LDI-MS measurements in positive ionization mode with sub-ppm mass accuracy (Table S3).

As depicted by the ion profiles shown in Figure 5, TOF-SIMS imaging of freshly toasted staves (t_0) showed a uniform distribution of polysaccharide fragment ions (*m/z* 31.02 *Δm* = -64.5 ppm, CH_3O^+ and *m/z* 97.03 *Δm* = -20.6 ppm, $C_5H_5O_2^+$) across the wood surface, which is also shown in the ion images in Figure S15.

However, in the 100-year-old staves (t_{100}), a significant decrease in polysaccharide fragment ion intensities was observed. Ion intensity profiles demonstrated a reduction from approximately 4 × 10^5 counts in the inner wall to around 1 × 10^5 counts in the outer regions of the stave (Figure 5). Theses ion profiles results were confirmed by TOF-SIMS imaging (Figure S15). This longitudinal gradient suggests that polysaccharide degradation occurs predominantly in the outer layers of the staves, likely due to prolonged environmental exposure (on the outside) and the continuous interaction with alcohol (in the inside) during barrel ageing. Thus, the degradation of polysaccharides can be attributed to multiple factors such as the role of alcohol extraction through time or hydrolytic degradation. For the first one, the high ethanol content in spirits may contribute to the dissolution and extraction of hemicellulose, leading to its gradual reduction over time. Moreover, the exposure to moisture, like fungi, and other environmental conditions over a century can result in the hydrolysis of polysaccharides, further diminishing their abundance in the aged stave.

The degradation of polysaccharides has critical implications for barrel ageing, as it can alter the wood porosity and influence the rate of oxygenation and interaction with the spirit. This, in turn, may affect the flavor profile of the spirit, as polysaccharides are known to contribute to sweetness.

Lipid Migration and Extraction, and triterpenoid

Lipids, including fatty acids and sterols, play a vital role in wood ageing and an important role in tree physiology, structure, and defense. The lipids detected by TOF-SIMS in oak heartwood are mainly fatty acids such as myristic acid at *m/z* 227.20 (*Δm* = 4.40 ppm) $[C_{14}H_{27}O_2]^-$, palmitoleic acid at *m/z* 253.21 (*Δm* = 11.8 pmm) $[C_{16}H_{29}O_2]^-$, palmitic acid at *m/z* 255.23 (*Δm* = -3.92 ppm) $[C_{16}H_{31}O_2]^-$, linoleic acid at *m/z* 279.23 (*Δm* = 10.7 ppm) $[C_{18}H_{31}O_2]^-$, oleic acid at *m/z* 281.25 (*Δm* = 3.56 ppm) $[C_{18}H_{33}O_2]^-$, lignoceric acid at *m/z* 367.36 (*Δm* = 8.17 ppm) $[C_{24}H_{47}O_2]^-$ and cerotic acid at *m/z* 395.39 (*Δm* = 12.6 ppm) $[C_{26}H_{51}O_2]^-$. Sterols were also detected such as the isomers of β-sitostenone at *m/z* 411.37 *Δm* = -7.29 ppm $[C_{29}H_{47}O]^-$, β-sitostenol at *m/z* 413.36 *Δm* = 50.8 ppm $[C_{29}H_{49}O]^-$ and the sterol $C_{29}H_{51}O_2$ at *m/z* 430.38 *Δm* = 16.3 ppm. Regarding the triterpenoids, these species were detected, as an example a quercotriterpenoside molecule was identified at *m/z* 817.40 *Δm* = 3.67 ppm, $[C_{43}H_{61}O_{15}]^-$.

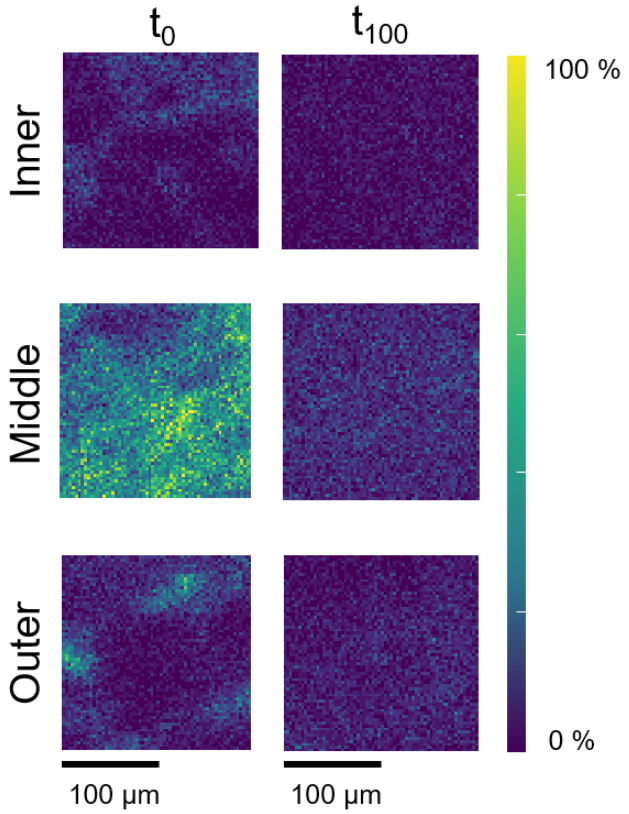

Figure 6: TOF-SIMS negative ion images of the sum of fatty acids (*m/z* 227.203; *m/z* 253.214; *m/z* 255.234; *m/z* 279.230; *m/z* 281.250; *m/z* 367.355; *m/z* 395.385) at the surface of cross-sections of staves from freshly toasted wood t_0, inner, middle, and outer, and historical wood t_{100}, inner, middle, and outer regions, recorded in High Current Bunched mode, image size 200 µm × 200 µm, 100 × 100-pixels, pixel size 2 µm, primary ion dose density 5.10^{11} ions.cm^{-2}.

The presence of fatty acids such as oleic acid was confirmed by LDI measurements with accurate mass (see Table S4). For sterols, no intact molecules could be detected in LDI (Table S3). This is most likely due to the non-polar nature of these compounds and the resulting low ionization efficiency under LDI conditions.

More specifically, by TOF-SIMS analysis, in freshly toasted staves (t_0), all the previously detected fatty acids were detected throughout the wood samples, with a higher intensity in the middle of the stave (Figure 6). In contrast, in the 100-year old staves (t_{100}), TOF-SIMS analysis revealed a significant decrease in the abundance of fatty acids. Moreover, residual lipids were detected around 8 mm from the inner wall of the stave, suggesting a potential lipid migration within the wood over time. This intensity may reflect a boundary where lipids are less accessible to extraction or may indicate a region of reorganization due to long-term alcohol contact. The reduction in lipid content, particularly in the outer layers, may also contribute to changes in the stave permeability, influencing oxygen exchange and the maturation process.

Phenolic Compounds and Transformation of Ellagitannins

Phenolic compounds detected by TOF-SIMS analysis include phenylacetaldehyde at *m/z* 121.06 *Δm* = 33.0 ppm $[C_8H_9O]^+$ and *m/z* 119.05 *Δm* = 8.40 ppm $[C_8H_7O]^-$, benzoic acid at *m/z* 123.04 *Δm* = 24.4 ppm $[C_7H_7O_2]^+$ and *m/z* 121.03 *Δm* = 16.5 ppm $[C_7H_5O_2]^-$, 4-hydroxybenzoic acid at *m/z* 139.04 *Δm* = -21.6 ppm $[C_7H_7O_3]^+$ and *m/z* 137.03 *Δm* = 7.30 ppm $[C_7H_5O_3]^-$, vanillin at *m/z* 153.06 *Δm* = −6.53 ppm $[C_8H_9O_3]^+$ and *m/z* 151.04

Δm = 13.2 ppm $[C_8H_7O_3]^-$, coniferyl aldehyde at *m/z* 179.07 Δm = -16.8 ppm $[C_{10}H_{11}O_3]^+$ and *m/z* 177.06 Δm = 5.65 ppm $[C_{10}H_9O_3]^-$, syringaldehyde at *m/z* 183.07 Δm = -38.2 ppm $[C_9H_{11}O_4]^+$ and *m/z* 181.05 Δm = 27.6 ppm $[C_9H_9O_4]^-$, sinapic acid at *m/z* 225.08 Δm = 4.44 ppm $[C_{11}H_{13}O_5]^+$ and *m/z* 223.06 Δm = 22.4 ppm $[C_{11}H_{11}O_5]^-$. The negative ionization mode allows the detection of some phenolic compounds, which are detected only in this mode as deprotonated molecules, but not detected in positive ion mode, such as protocatechuic acid at *m/z* 153.02 Δm = 13.1 ppm $[C_7H_5O_4]^-$; vanillic acid at *m/z* 167.04 Δm = −5.99 ppm $[C_8H_7O_4]^-$; gallic acid at *m/z* 169.01 Δm = 5.92 ppm $[C_7H_5O_5]^-$; caffeic acid at *m/z* 179.03 Δm = 22.3 ppm $[C_9H_7O_4]^-$. This agrees with the TOF-SIMS reference mass spectra, where the intensities of peaks of the deprotonated molecules are often about 10 times greater that the intensities of the protonated ones. [36,37,38,39] Among the polyphenolic compounds in oak, coumarins are also detected, which are compounds known to act in plant defense against pathogens and providing protection against UV light. The aglycone coumarin at *m/z* 145.03 Δm = 20.7 ppm $[C_9H_5O_2]^-$; umbelliferone at *m/z* 161.03 Δm = -43.5 ppm $[C_9H_5O_3]^-$; 4-methylumbelliferone at *m/z* 177.06 Δm = 5.65 ppm $[C_{10}H_9O_3]^-$; aesculetin at *m/z* 177.01 Δm = 28.2 ppm $[C_9H_5O_4]^-$; scopoletin at *m/z* 191.03 Δm = 664 ppm $[C_{10}H_7O_4]^-$. All *m/z* mentioned above were confirmed by LDI measurements in negative mode with high mass accuracy (see Table S4). Several of them, but not all, were also detected in positive ionization mode (see Table S3). Other polyphenolic compounds were detected using TOF-SIMS such as tergallic acid at *m/z* 507.09 Δm = -92.7 ppm $[C_{21}H_{15}O_{15}]^+$ and *m/z* 505.03 Δm = -9.90 ppm $[C_{21}H_{13}O_{15}]^-$; castalin at *m/z* 631.07 Δm = -17.4 ppm $[C_{27}H_{19}O_{18}]^-$; pedunculagin at *m/z* 783.07 Δm = 2.55 ppm $[C_{34}H_{23}O_{22}]^-$; castalagin or its isomer vescalagin at *m/z* 935.09 Δm = -15.0 ppm $[C_{41}H_{27}O_{26}]^+$, *m/z* 957.07 Δm = 5.22 ppm $[C_{41}H_{26}O_{26}Na]^+$, *m/z* 973.02 Δm = 13.4 ppm $[C_{41}H_{26}O_{26}K]^+$ and *m/z* 933.08 Δm = 12.9 ppm $[C_{41}H_{25}O_{26}]^-$. The latter are belonging to ellagitannins, which are a unique group of hydrolysable tannins that can be found in oak wood. They play a key role in protecting the wood from decay, thus contributing significantly to the flavor profile of aged spirits. Ellagic acid was identified according to its reference mass spectra previously analyzed by TOF-SIMS[36,37,38,39], in addition of the other ellagitannins, at *m/z* 303.01 Δm = 16.5 ppm $[C_{14}H_7O_8]^+$ and *m/z* 300.999 Δm = 0 ppm $[C_{14}H_5O_8]^-$. This molecule is at the same time the result of gallic acid dimerization and a specific degradation product of the ellagitannins class, and was detected in both t_0 and t_{100} staves. According to the intensity profiles of this ion along the staves (Figure S19), the relative stability of ellagic acid suggests that it persists throughout the ageing process, contributing to the astringency and bitterness of the spirits. It was also confirmed by LDI measurements in positive and negative ionization mode (see Table S3 and Table S4).

It can be noted that TOF-SIMS imaging revealed a change in the distribution of ellagitannins between the t_0 and t_{100} staves. In the freshly toasted wood, ellagitannins were homogeneously distributed from the middle to the inner stave wall, while in the aged wood, they were found specifically localized inside the fibers of the middle and inner surface (Figure 7). This suggests that ellagitannins undergo gradual degradation[17] and diffusion deeper into the stave fibers during the ageing process, likely facilitated by the breakdown of larger tannin molecules into smaller phenolic compounds such as ellagic acid.

This change in the spatial distribution of ellagitannins may be influenced by several factors, including thermal degradation during the toasting process leading to a possible breakdown of the tannins, thus resulting in the formation of smaller phenolic compounds. The microbial interactions with environmental fungi during barrel ageing could also contribute to the molecule breakdown and migration of degradation fragments through the stave.

The redistribution of ellagitannins may have significant implications for the flavor of aged spirits[17]. As these compounds degrade and migrate, they continue to contribute to the chemical composition of the spirits, potentially influencing astringency and bitterness in the final product.

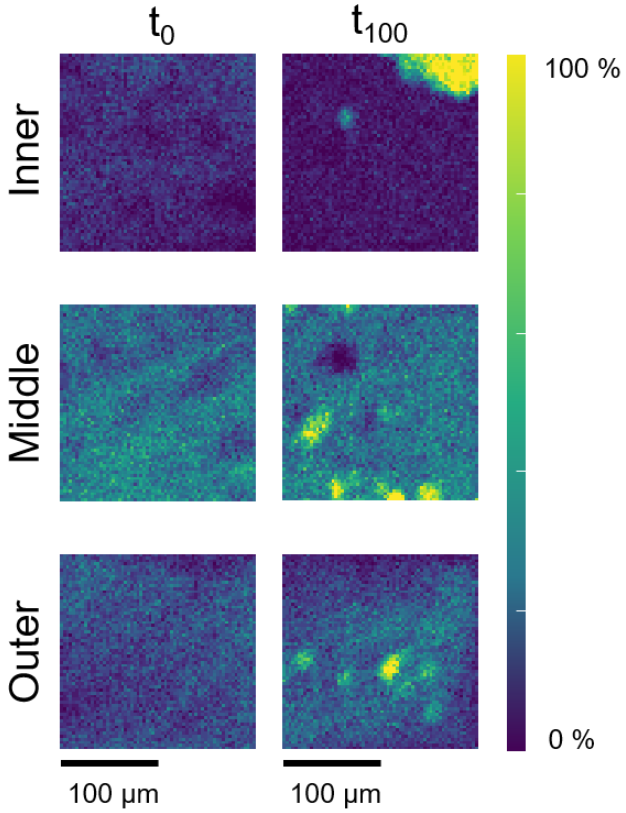

Figure 7: TOF-SIMS image of ellagic acid anion (m/z 300.999) at the surface of stave cross sections from freshly toasted wood t0, inner, middle, and outer and historical wood t100, inner, middle, and outer regions, recorded in High Current Bunched mode, image size 200 µm × 200 µm, 100 × 100-pixels, pixel size 2 µm, primary ion dose density 5.1011 ions.cm^{-2}.

CONCLUSIONS

This study used LC-MS/MS, LDI-MS and TOF-SIMS analyses to gain a clearer picture of the chemical changes in oak wood during the long-term ageing of Cognac spirits. By examining how compounds can migrate and transform over time, we identified some of the main factors that could influence the flavor of the aged spirits. The stability of lignins through time suggests that these compounds play a key role in keeping the wood structure. In contrast, polysaccharides contained in the wood tend to break down over time, and more specifically in the outer layers of the wood. This is likely due to environmental exposure and contact with alcohol, and it can impact the wood structure and thus the amount of oxygen flowing through it, leading to a change in the sweetness or to the texture of the aged spirit. The migration and transformation of ellagitannins in the wood show that these class of molecules always have an influence on the spirit astringency and bitterness over time. Indeed, while the barrel toasting releases a significant part of these

compounds, the long-term alcohol contact induces the formation of breakdown products, thus adding more complexity to the final taste of the spirit. The lipids which are contained in the wood, such as fatty acids, gradually potentially migrate into the spirit, where they can affect its texture or its taste. This hypothesis could be verified by comparisons with analyses on the cognac spirit at different ageing stages. We also found that some lipids remain in the inner layers of the wood, potentially acting as a reservoir that will release aroma compounds through time and exposure. Using TOF-SIMS, LDI-MS and LC-MS/MS as complementary approaches allowed us to highlight these complex changes, thus helping us to better understand the interactions between wood barrels and alcohol along time.

ASSOCIATED CONTENT

Supporting Information

LC-MS/MS analysis annotation of oak wood compound using t-SNE molecular networking visualization are included. Detailed of polysaccharides, lignin, and ellagic acid distribution profiles, plus cellulose, xylan and lignin ion images obtained by TOF-SIMS analysis are provided. An LDI-MS spectrum in positive ionization mode is also provided. Moreover, tables containing all annotated compounds by LC-MS/MS, TOF-SIMS and LDI-MS are also provided (Figures S1 – S20 and Tables S1 – S6).

AUTHOR INFORMATION

Corresponding Author

* **Alain Brunelle** – Laboratoire d'Archéologie Moléculaire et Structurale, LAMS UMR8220, CNRS, Sorbonne Université 75005 Paris, France ; orcid.org/0000-0001-6526-6481
Email: alain.brunelle@cnrs.fr

Present Addresses

†Institut Pasteur 25-28 rue du Dr Roux, 75015 Paris

Author Contributions

+ A.C. and Q.P.V. contributed equally.
The manuscript was written through contributions of all authors.
All authors have given approval to the final version of the manuscript.

Notes

The authors declare no competing financial interest.

ACKNOWLEDGMENTS

Thiéry Guillou is kindly acknowledged for crafting with meticulous attention to detail the TOF-SIMS sample holders with a vise-like mechanism. We would like to thank Julia Kokesch-Himmelreich and Grace Odedina for support in processing of the LDI-MS data. This work was financially supported by the Agence Nationale de la Recherche (grant ANR-21-CE29-0026 MULTI-ANGEL-MSI), Deutsche Forschungsgemeinschaft (RO 3421/8-1 and INST 91 373-1 FUGG), and by the DIM PAMIR (IDF-DIM-PAMIR-2023-4-001 ANGELSHARE).

REFERENCES

(1) Mosedale, J. R. Effects of Oak Wood on the Maturation of Alcoholic Beverages with Particular Reference to Whisky. *Forestry* **1995**, *68* (3), 203–230. https://doi.org/10.1093/forestry/68.3.203.

(2) Mosedale, J. R.; Puech, J. L. Wood Maturation of Distilled Beverages. *Trends Food Sci. Technol.* **1998**, *3* (9), 95–101. https://doi.org/10.1016/s0924-2244(98)00024-7.

(3) Guerrero-Chanivet, M.; Valcárcel-Muñoz, M. J.; García-Moreno, M. V.; Guillén-Sánchez, D. A. Characterization of the Aromatic and Phenolic Profile of Five Different Wood Chips Used for Ageing Spirits and Wines. *Foods* **2020**, *9* (11), 1613. https://doi.org/10.3390/foods9111613.

(4) Tarko, T.; Krankowski, F.; Duda-Chodak, A. The Impact of Compounds Extracted from Wood on the Quality of Alcoholic Beverages. *Molecules* **2023**, *28* (2), 620. https://doi.org/10.3390/molecules28020620.

(5) *Wood Chemistry and Wood Biotechnology*; Ek, M., Gellerstedt, G., Henriksson, G., Eds.; Walter de Gruyter, 2009. https://doi.org/10.1515/9783110213409.

(6) Nonier, M.-F.; Vivas, N.; Gaulejac, N. V. de; Fouquet, E. Origin of brown discoloration in the staves of oak used in cooperage – Characterization of two new lignans in oak wood barrels. *Comptes Rendus Chim.* **2009**, *12* (1–2), 291–296. https://doi.org/10.1016/j.crci.2008.04.004.

(7) Ghadiriasli, R.; Wagenstaller, M.; Buettner, A. Identification of Odorous Compounds in Oak Wood Using Odor Extract Dilution Analysis and Two-Dimensional Gas Chromatography-Mass Spectrometry/Olfactometry. *Anal. Bioanal. Chem.* **2018**, *410* (25), 6595–6607. https://doi.org/10.1007/s00216-018-1264-7.

(8) Vivas, N.; Glories, Y. Role of Oak Wood Ellagitannins in the Oxidation Process of Red Wines During Aging. *Am. J. Enol. Vitic.* **1996**, *47* (1), 103–107. https://doi.org/10.5344/ajev.1996.47.1.103.

(9) Gadrat, M.; Lavergne, J.; Emo, C.; Teissedre, P.-L.; Chira, K. Validation of a Mass Spectrometry Method to Identify and Quantify Ellagitannins in Oak Wood and Cognac during Aging in Oak Barrels. *Food Chem.* **2021**, *342*, 128223. https://doi.org/10.1016/j.foodchem.2020.128223.

(10) Brunelle, A.; Touboul, D.; Laprévote, O. Biological Tissue Imaging with Time-of-Flight Secondary Ion Mass Spectrometry and Cluster Ion Sources. *J. Mass Spectrom.* **2005**, *40* (8), 985–999. https://doi.org/10.1002/jms.902.

(11) Vanbellingen, Q. P.; Elie, N.; Eller, M. J.; Della-Negra, S.; Touboul, D.; Brunelle, A. Time-of-Flight Secondary Ion Mass Spectrometry Imaging of Biological Samples with Delayed Extraction for High Mass and High Spatial Resolutions. *Rapid Commun. Mass Spectrom.* **2015**, *29* (13), 1187–1195. https://doi.org/10.1002/rcm.7210.

(12) Vanbellingen, Q. P.; Fu, T.; Bich, C.; Amusant, N.; Stien, D.; Della-Negra, S.; Touboul, D.; Brunelle, A. Mapping Dicorynia Guianensis Amsh. Wood Constituents by Submicron Resolution Cluster-TOF-SIMS Imaging. *J. Mass Spectrom.* **2016**, *51* (6), 412–423. https://doi.org/10.1002/jms.3762.

(13) Chambers, M. C.; Maclean, B.; Burke, R.; Amodei, D.; Ruderman, D. L.; Neumann, S.; Gatto, L.; Fischer, B.; Pratt, B.; Egertson, J.; Hoff, K.; Kessner, D.; Tasman, N.; Shulman, N.; Frewen, B.; Baker, T. A.; Brusniak, M.-Y.; Paulse, C.; Creasy, D.; Flashner, L.; Kani, K.; Moulding, C.; Seymour, S. L.; Nuwaysir, L. M.; Lefebvre, B.; Kuhlmann, F.; Roark, J.; Rainer, P.; Detlev, S.; Hemenway, T.; Huhmer, A.; Langridge, J.; Connolly, B.; Chadick, T.; Holly, K.; Eckels, J.; Deutsch, E. W.; Moritz, R. L.; Katz, J. E.; Agus, D. B.; MacCoss, M.; Tabb, D. L.; Mallick, P. A Cross-Platform Toolkit for Mass Spectrometry and Proteomics. *Nat. Biotechnol.* **2012**, *30* (10), 918–920. https://doi.org/10.1038/nbt.2377.

(14) Schmid, R.; Heuckeroth, S.; Korf, A.; Smirnov, A.; Myers, O.; Dyrlund, T. S.; Bushuiev, R.; Murray, K. J.; Hoffmann, N.; Lu, M.; Sarvepalli, A.; Zhang, Z.; Fleischauer, M.; Dührkop, K.; Wesner, M.; Hoogstra, S. J.; Rudt, E.; Mokshyna, O.; Brungs, C.; Ponomarov, K.; Mutabdžija, L.; Damiani, T.; Pudney, C. J.; Earll, M.; Helmer, P. O.; Fallon, T. R.; Schulze, T.; Rivas-Ubach, A.; Bilbao, A.; Richter, H.; Nothias, L.-F.; Wang, M.; Orešič, M.; Weng, J.-K.; Böcker, S.; Jeibmann, A.; Hayen, H.; Karst, U.; Dorrestein, P. C.; Petras, D.; Du, X.; Pluskal, T. Integrative Analysis of Multimodal Mass Spectrometry Data in MZmine 3. *Nat. Biotechnol.* **2023**, *41* (4), 447–449. https://doi.org/10.1038/s41587-023-01690-2.

(15) Olivon, F.; Elie, N.; Grelier, G.; Roussi, F.; Litaudon, M.; Touboul, D. MetGem Software for the Generation of Molecular Networks Based on the T-SNE Algorithm. *Anal. Chem.* **2018**, *90* (23), 13900–13908. https://doi.org/10.1021/acs.analchem.8b03099.

(16) Díaz-Maroto, M. C.; Guchu, E.; Castro-Vázquez, L.; de Torres, C.; Pérez-Coello, M. S. Aroma-Active Compounds of American, French, Hungarian and Russian Oak Woods, Studied by GC–MS

and GC–O. *Flavour Fragr. J.* **2008**, *23* (2), 93–98. https://doi.org/10.1002/ffj.1859.
(17) Viriot, Carole.; Scalbert, Augustin.; Lapierre, Catherine.; Moutounet, Michel. Ellagitannins and Lignins in Aging of Spirits in Oak Barrels. *J. Agric. Food Chem.* **1993**, *41* (11), 1872–1879. https://doi.org/10.1021/jf00035a013.
(18) Puech, J. L.; Moutounet, M. Liquid Chromatographic Determination of Scopoletin in Hydroalcoholic Extract of Oak Wood and in Matured Distilled Alcoholic Beverages. *J. - Assoc. Off. Anal. Chem.* **1988**, *71* (3), 512–514.
(19) Setzer, W. N. Volatile Components of Oak and Cherry Wood Chips Used in Aging of Beer, Wine, and Sprits.
(20) Rasines-Perea, Z.; Jacquet, R.; Jourdes, M.; Quideau, S.; Teissedre, P.-L. Ellagitannins and Flavano-Ellagitannins: Red Wines Tendency in Different Areas, Barrel Origin and Ageing Time in Barrel and Bottle. *Biomolecules* **2019**, *9* (8), 316. https://doi.org/10.3390/biom9080316.
(21) Venter, P.; Causon, T.; Pasch, H.; de Villiers, A. Comprehensive Analysis of Chestnut Tannins by Reversed Phase and Hydrophilic Interaction Chromatography Coupled to Ion Mobility and High Resolution Mass Spectrometry. *Anal. Chim. Acta* **2019**, *1088*, 150–167. https://doi.org/10.1016/j.aca.2019.08.037.
(22) Hayasaka, Y.; Wilkinson, K. L.; Elsey, G. M.; Raunkjær, M.; Sefton, M. A. Identification of Natural Oak Lactone Precursors in Extracts of American and French Oak Woods by Liquid Chromatography–Tandem Mass Spectrometry. *J. Agric. Food Chem.* **2007**, *55* (22), 9195–9201. https://doi.org/10.1021/jf072171u.
(23) Masson, E.; Baumes, R.; Le Guernevé, C.; Puech, J.-L. Identification of a Precursor of β-Methyl-γ-Octalactone in the Wood of Sessile Oak (Quercus Petraea (Matt.) Liebl.). *J. Agric. Food Chem.* **2000**, *48* (9), 4306–4309. https://doi.org/10.1021/jf0002950.
(24) Vidlar, M.; Dadakova, K.; Kasparovsky, T.; Baron, M.; Průšová, B.; Sochor, J. Study of Lignans in Wine Originating from Different Types of Oak Barrels. *OENO One* **2023**, *57* (3), 233–242. https://doi.org/10.20870/oeno-one.2023.57.3.7128.
(25) Sanz, M.; de Simón, B. F.; Cadahía, E.; Esteruelas, E.; Muñoz, A. M.; Hernández, T.; Estrella, I.; Pinto, E. LC-DAD/ESI-MS/MS Study of Phenolic Compounds in Ash (Fraxinus Excelsior L. and F. Americana L.) Heartwood. Effect of Toasting Intensity at Cooperage. *J. Mass Spectrom.* **2012**, *47* (7), 905–918. https://doi.org/10.1002/jms.3040.
(26) Cretin, B. N.; Dubourdieu, D.; Marchal, A. Development of a Quantitation Method to Assay Both Lyoniresinol Enantiomers in Wines, Spirits, and Oak Wood by Liquid Chromatography-High Resolution Mass Spectrometry. *Anal. Bioanal. Chem.* **2016**, *408* (14), 3789–3799. https://doi.org/10.1007/s00216-016-9466-3.
(27) Li, H.; Ding, X.; An, Q.; Li, W.; Guo, L.; Zheng, Y.; Zhang, D.; Huo, W. A Strategy Comprehensively and Quickly Identifies the Herbal Composition and Chemical Constituents in Yixishu Lotion by Molecular Networking. *Biomed. Chromatogr.* **2025**, *39* (5), e70069. https://doi.org/10.1002/bmc.70069.
(28) Fernández de Simón, B.; Esteruelas, E.; Muñoz, Á. M.; Cadahía, E.; Sanz, M. Volatile Compounds in Acacia, Chestnut, Cherry, Ash, and Oak Woods, with a View to Their Use in Cooperage. *J. Agric. Food Chem.* **2009**, *57* (8), 3217–3227. https://doi.org/10.1021/jf803463h.
(29) Gammacurta, M.; Waffo-Teguo, P.; Winstel, D.; Cretin, B. N.; Sindt, L.; Dubourdieu, D.; Marchal, A. Triterpenoids from Quercus Petraea: Identification in Wines and Spirits and Sensory Assessment. *J. Nat. Prod.* **2019**, *82* (2), 265–275. https://doi.org/10.1021/acs.jnatprod.8b00682.
(30) Pérez, A. J.; Pecio, Ł.; Kowalczyk, M.; Kontek, R.; Gajek, G.; Stopinsek, L.; Mirt, I.; Oleszek, W.; Stochmal, A. Triterpenoid Components from Oak Heartwood (Quercus Robur) and Their Potential Health Benefits. *J. Agric. Food Chem.* **2017**, *65* (23), 4611–4623. https://doi.org/10.1021/acs.jafc.7b01396.
(31) Mahato, S. B.; Nandy, A. K.; Kundu, A. P. Pentacyclic Triterpenoid Sapogenols and Their Glycosides from Terminalia Bellerica<math><mtext>terminalia Bellerica</Mtext></Math>. *Tetrahedron* **1992**, *48* (12), 2483–2494. https://doi.org/10.1016/S0040-4020(01)88767-6.
(32) Rao, G. S. R. S.; Prasanna, S.; Kumar, V. P. S.; Mallavarapu, G. R. Bartogenic Acid, a New Triterpene Acid from *Barringtonia Speciosa*. *Phytochemistry* **1981**, *20* (2), 333–334. https://doi.org/10.1016/0031-9422(81)85119-9.
(33) Vanbellingen, Q. Imagerie de substances naturelles par spectrométrie de masse, Ph.D. thesis, Paris-Saclay University, 2015, https://theses.hal.science/tel-01278744.
(34) Goacher, R. E.; Jeremic, D.; Master, E. R. Expanding the Library of Secondary Ions That Distinguish Lignin and Polysaccharides in Time-of-Flight Secondary Ion Mass Spectrometry Analysis of Wood. *Anal. Chem.* **2011**, *83* (3), 804–812. https://doi.org/10.1021/ac1023028.
(35) Saito, K.; Kato, T.; Tsuji, Y.; Fukushima, K. Identifying the Characteristic Secondary Ions of Lignin Polymer Using ToF-SIMS. *Biomacromolecules* **2005**, *6 2*, 678–683. https://doi.org/10.1021/BM049521V.
(36) Cournut, A.; Belhachmi, S.; Bouvier, C.; Brunelle, A. TOF-SIMS spectra of gallic acid, ellagic acid, castalin, and quercetin in negative polarity. *Submitted to Surf. Sci. Spectra*.
(37) Cournut, A.; Belhachmi, S.; Bouvier, C.; Brunelle, A. TOF-SIMS spectra of gallic acid, ellagic acid, castalin, and in positive polarity. *Submitted to Surf. Sci. Spectra*.
(38) Cournut, A.; Belhachmi, S.; Bouvier, C.; Brunelle, A. TOF-SIMS spectra of caffeic acid, vanillin, eugenol, and cellulose in negative polarity. *Submitted to Surf. Sci. Spectra*.
(39) Cournut, A.; Belhachmi, S.; Bouvier, C.; Brunelle, A. TOF-SIMS spectra of caffeic acid, vanillin, eugenol, and cellulose in positive polarity. *Submitted to Surf. Sci. Spectra*.